Study of microstructure, hardness and thermal properties of Sn-Bi alloys

Kristina N. Božinović, Dragan M. Manasijević, Ljubiša T. Balanović, Milan D. Gorgievski, Uroš S. Stamenković, Miljan S. Marković and Zoran D. Mladenović

Technical Faculty in Bor, Department of Metallurgical Engineering, University of Belgrade, Vojske Jugoslavije 12, 19210 Bor, Serbia

Abstract

Lead-free solders have become a main focus of the electronic industry in recent years, because of the high toxicity of lead. Alloys based on the Sn-Bi system figure as potential replacements for Sn-Pb alloys in soldering due to favorable properties and low cost. One of the main advantages of these alloys are low melting temperatures, while additional advantages include good compatibility with substrates, low process temperature, high reliability, and potential applications in conjunction with reduced graphene oxide nanosheets as thermal interface materials. In this paper, characterization of microstructural and thermal properties as well as hardness measurements of seven alloys of different Sn-Bi compositions are performed. Structural properties of the samples were analyzed using optical microscopy and scanning electron microscopy and energy dispersive X-ray spectroscopy (SEM-EDS). Thermal conductivity of the samples was investigated using the xenon-flash method, and phase transition temperatures were measured using the differential scanning calorimetry (DSC) analysis.

Keywords: structural properties; soldering; lead-free solders; thermal conductivity.

Available on-line at the Journal web address: http://www.ache.org.rs/HI/

ORIGINAL SCIENTIFIC PAPER

UDC: 620.17:669.017.12 (546.811+546.87)

Hem. Ind. **75 (4)** 227-239 (2021)

1. INTRODUCTION

For a long time, lead-tin alloy was broadly used in electronic industry because of its favorable physical and mechanical characteristics (low melting point, good wettability on different substrates, high strength of joints), and well-studied and optimized production [1]. Because of the high toxicity of lead, this alloy was abandoned, which prompted the electronics industry to seek for new solutions and lead-free solders became one of the main interests. A variety of systems have been proposed such as Sn-Ag, Sn-Cu, Sn-Bi, Sn-Zn, Sn-Au, Sn-Ag-Cu (SAC), Sn-Bi-Zn, Sn-Ag-Cu-Bi, etc. [2-5]. Commonly used in wave and reflow soldering processes, many of these lead-free solders melt at much higher temperatures than the conventional Sn-Pb eutectic solder (183°C). Higher melting temperatures cause damage to high-temperature-sensitive components and pose a major challenge to the electronic industry [4-5]. Alloys based on the Sn-Bi system were proposed as one of the best candidates in replacing Sn-Pb alloys in soldering due to their low melting temperatures (eutectic point: 139°C), good mechanical properties and cost-efficiency [1,5-8]. Yet, Sn-Bi solder alloys have also disadvantages, such as precipitation of Bi in the supersaturated Sn matrix during aging, and coarsening of the microstructure in the case of Bi-rich phases [9,10]. Therefore, a considerable number of investigations have been devoted to examining microstructure and mechanical properties of Sn-Bi alloys with addition of alloying elements such as Ni, Cu, Zn, Ag [5,6,9-14]. These systems with addition of other components also, have been particularly researched because of their potential application as thermal interface materials (TIM). The increasing demand for higher processing speeds, and smaller and thinner products had led the electronic industry to develop high performance devices, leaving a thermal management as a main challenge. In microelectronic packaging, TIM acts as a tunnel for the heat transfer from the device to the heat sink. Simultaneously, it provides a mechanical connection. The efficiency of the thermal management system is largely limited by the thermal conductivity of the TIM. Sn-Bi alloys reinforced with carbon

Corresponding author: Kristina N. Božinović, Technical Faculty in Bor, Department of Metallurgical Engineering, University of Belgrade, Vojske Jugoslavije 12, 19210 Bor, Serbia; tel. +381 61 613 12 95

E-mail: kbozinovic@tfbor.bg.ac.rs

Paper received: 19 January 2021; Paper accepted: 09 July 2021; Paper published: 30 July, 2021

https://doi.org/10.2298/HEMIND210119021B

nanotubes, reduced graphene oxide nanosheets, and other supplements have become very attractive as TIMs, because of their relatively low process temperatures, high reliability, and good compatibility with substrates [15-18].

In recent years, research of Sn-Bi system properties has been mainly focused on microstructure [9,19-24], mechanical properties [9,12,13,20-23], wettability [25,26], thermal characteristics [20,27], and interfacial reactions between the molten solder and the substrate [24,28], considering primarily the Sn-Bi eutectic alloy. Very little to none attention was given to the thermal conductivity [20,29] and hardness measurements. Therefore, this work focused on microstructure characterization, hardness measurements, and thermal properties investigations as a contribution to more complete knowledge of the mentioned system. These investigations included determination of thermal diffusivities and thermal conductivities of seven Sn-Bi alloys with different compositions.

2. EXPERIMENTAL

The metals used for the preparation of selected samples were bismuth and tin of >99.9 % purity (Alfa Aesar, United States). The investigated alloys with bismuth molar fractions of 0.1; 0.2; 0.4; 0.5; 0.6; 0.8 and 0.9 were prepared by melting weighted masses of pure metals in alumina crucibles under inert argon atmosphere at 400°C. The investigated compositions are given in Table 1.

Table 1. Molar and mass compositions of investigated Sn-Bi alloys

	x		Content, mas.%	
Sample	**Bi**	**Sn**	**Bi**	**Sn**
Alloy 1	0.1	0.9	16.36	83.64
Alloy 2	0.2	0.8	30.56	69.44
Alloy 3	0.4	0.6	53.99	46.01
Alloy 4	0.5	0.5	63.77	36.23
Alloy 5	0.6	0.4	72.53	27.47
Alloy 6	0.8	0.2	87.56	12.44
Alloy 7	0.9	0.1	94.06	5.97

After solidification of alloy ingots, they were further homogenized for 60 min at 120 °C and cut into two parts. A smaller part of the sample was used for differential scanning calorimetry (DSC) analysis, and the remaining part was pressed by a hydraulic press (Mohr-Federhaff-Losenhausen, Germany) to obtain samples of the same dimensions in form of a tablet 12.7 mm in diameter and about 2 mm thick. The pressing force was 7000 N.

Annealing was performed after pressing in order to remove internal stresses created during the pressing. The annealing was carried out at 100 °C, in a closed chamber furnace, in a nitrogen-protected atmosphere, for 6 h.

Pressed and annealed samples were then used for investigations of thermal conductivity and diffusivity, structural analyses, and hardness measurements.

The samples were prepared for the microstructural investigation *via* three steps: grinding, polishing and structure development. In the structure development step, different etching agents were used, depending on the composition (5 % alcoholic solution of hydrochloric acid – 5 % HCl in C_2H_5OH; A solution of ferric chloride in water - $FeCl_3$ + HCl in H_2O; concentrated nitric acid - conc. HNO_3; 8 % hydrochloric acid solution in alcohol – 8 % HCl in C_2H_5OH). All chemicals used as etching agents were GR graded and produced by Dispochem.

Investigation of microstructural properties was performed by using light optical microscopy (LOM, Carl Zeiss Jena Epy Type 2 microscope, Zeiss, Germany) as well as by scanning electron microscopy and energy dispersive X-ray spectroscopy (SEM-EDS, VEGA 3, TESCAN, USA). Phase transition temperatures were measured by using the DSC analysis (SDT-Q600 Simultaneous TGA/DSC, TA Instruments, Germany), and thermal conductivities of the investigated alloys were determined by using the xenon-flash method on TA Discovery Xenon Flash (DXF) 500 instrument (TA Instruments, Germany). The experimental procedure is explained in detail in the previous paper [30].

The investigation of hardness was also carried out using Brinell's method (HPO 250, WPM Leipzig, Germany) with the applied force of 50 N. The measurements were performed at three different points of the sample surface, and the mean value was calculated.

Thermal analysis was conducted on the DSC/DTA/TGA simultaneous device TA SDT Q600 (TA Instruments, Germany). The specimens with an approximate weight of 40 mg were heated to 350 °C under inert argon atmosphere, at a constant rate of 5 °C/min. The onset temperature of the first DSC peak in the heating process was considered as the temperature of the eutectic reaction, and the peak temperature of the second thermal effect on heating was selected as the liquidus temperature.

3. RESULTS AND DISCUSSION

3. 1. Results of LOM and SEM-EDS analysis

The samples were prepared *via* three steps: grinding, polishing and structure development and afterwards examined by using the optical microscope (Fig. 1).

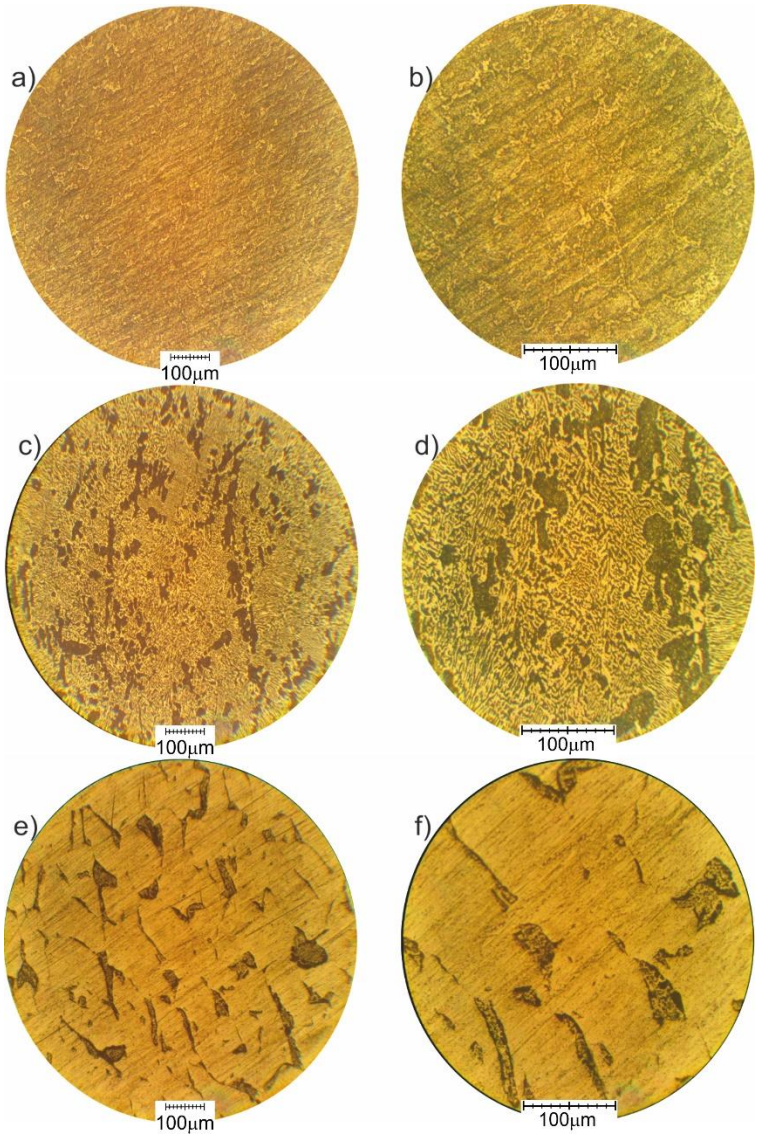

Fig. 1. Optical micrographs of chosen samples: (a) Alloy 2 magnification 200×; (b) Alloy 2 magnification 500×; (c) Alloy 3 magnification 200×; (d) Alloy 3 magnification 500×; (e); Alloy 7 magnification 200×; (f) Alloy 7 magnification 500×

Existence of two phases can be distinguished in the presented results as well as by the SEM-EDS analysis (Fig. 2). In Figure 1 darker areas correspond to the phase richer in tin and brighter to the phase richer in bismuth. However, in Figure 1c and d the eutectic mixture present in the microstructure can be observed. SEM-EDS analysis was used to analyze the phase morphology, to identify the coexisting phases, and to determine sample compositions (both overall and phase compositions).

For the alloys analyzed by using SEM (Fig. 2), co-existing phases in the microstructure were confirmed by the EDS point analysis. In the obtained SEM micrographs presented in Figures 3, 4 and 5 the darker colour signifies the phase richer in the lighter metal tin, and the brighter colour, on the other hand, corresponds to the phase richer in the heavier metal bismuth.

In this case, the existence of two phases is explained by the presence of a solid solution based on bismuth and a solid solution based on tin, which was confirmed by the EDS analysis.

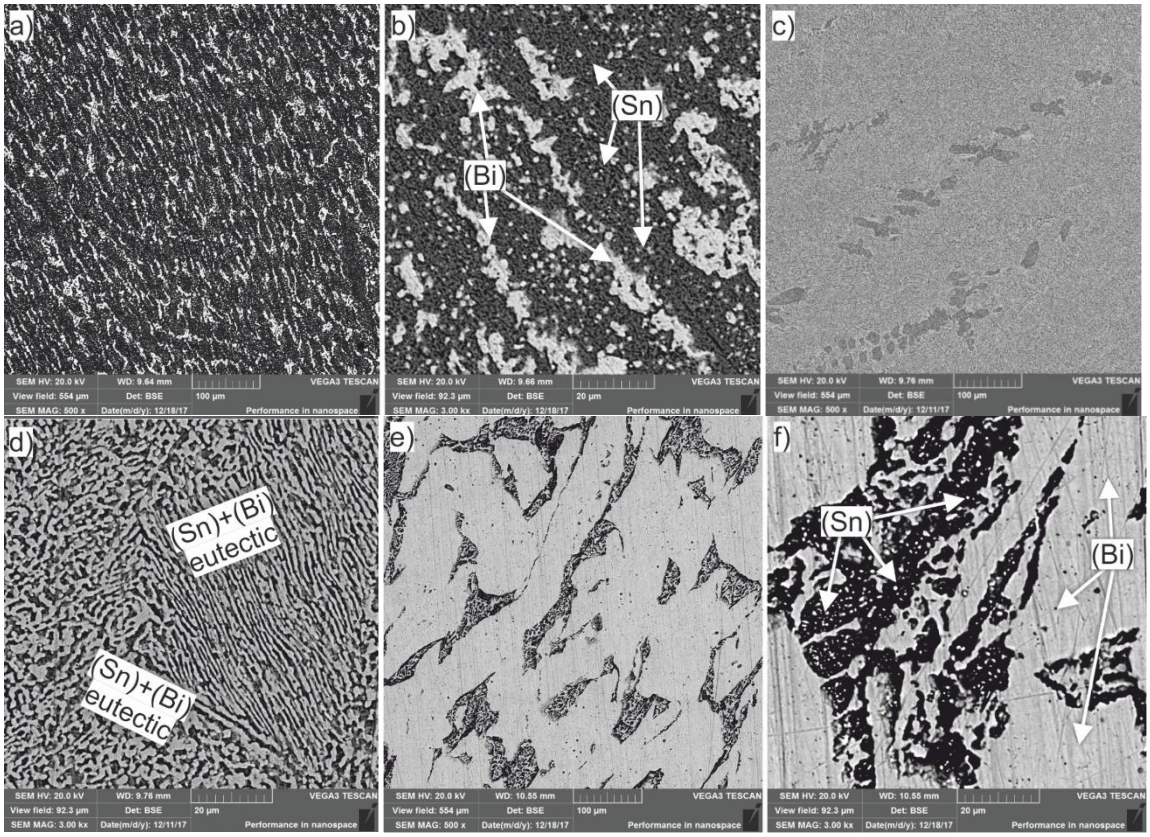

Fig. 2. SEM micrographs of examined samples - mixture of light (Bi) and dark (Sn) phases: a) Alloy 2 magnification 500×; (b) Alloy 2 magnification 3000×; (c) Alloy 3 magnification 500×; (d) Alloy 3 magnification 3000×; (e) Alloy 6 magnification 500×; (f) Alloy 6 magnification 3000×

We performed two types of the EDS analysis: 1) testing the overall composition of the observed surface and 2) examining the composition at individual points or spectrums on the surface.

Numerical values obtained by both types of EDS analysis, shown as atomic percentages of investigated components, are shown in Tables 2, 3 and 4, for each sample individually. Figure 3 shows microstructure of the Sn-rich sample, the alloy 2 (Bi0.2Sn0.8) subjected to the SEM-EDS analysis where Figure 3a shows the surface at which the overall composition was determined while Figure 3b shows particular points at which individual spectrums were obtained.

As it is shown in Figure 3b and in Table 2, darker phase represents the phase rich in tin solid solution (spectra 3 and 4), and lighter phase represents the phase rich in bismuth solid solution (spectra 1 and 2). In dark regions Sn-rich dendrites with Bi precipitates inside can be seen. A good agreement between the overall composition of the investigated surface and the nominal composition of the alloy 2 is obtained.

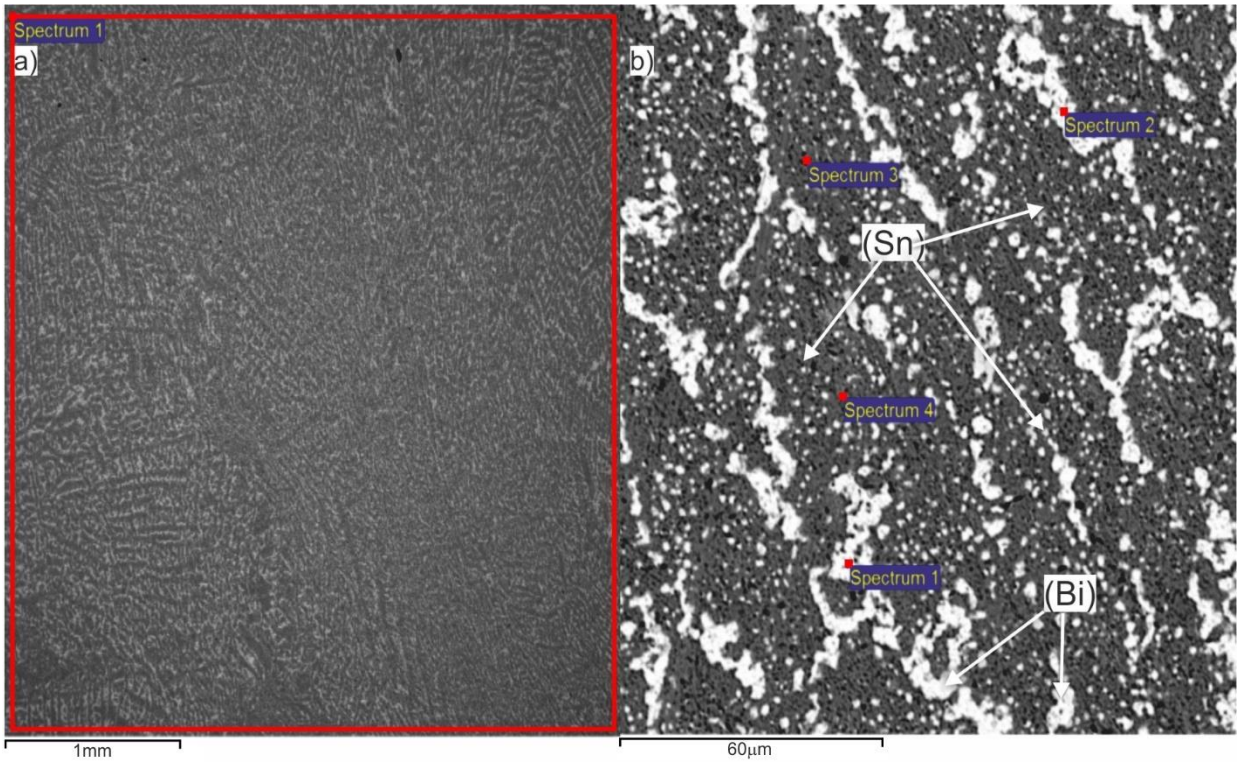

Fig. 3. SEM-EDS micrographs of the alloy 2 (Bi0.2Sn0.8): (a) determination of the overall composition; (b) determination of composition based on spectrums obtained at four different spots .

Table 2. Results of EDS spectrum analyses for the alloy 2 (Bi0.2Sn0.8)

Nominal composition of alloys, at.%		Overall composition of the observed surface, at.%		Identified phase	Individual point spectrum	Content, at.%	
						Sn	Bi
Bi	Sn	Bi	Sn	(Bi)	Spectrum 1	2.17	97.83
					Spectrum 2	3.40	96.60
20.00	80.00	19.82	80.18	(Sn)	Spectrum 3	96.48	3.52
					Spectrum 4	90.09	9.91

Fig. 4 represents the results of the SEM-EDS analysis for the near-eutectic sample, alloy 3 (Bi0.4Sn0.6) where the overall microstructure and details of the eutectic microstructure under higher magnification are shown.

Table 3 shows good agreement between the chemical composition of the examined surface and the nominal alloy composition. The Bi–Sn eutectic has an irregular lamellar structure, also termed a complex regular microstructure in which two phases are arranged in alternating not-flat plates [20]. This eutectic microstructure arrangement is also recognized as a “Chinese script” eutectic structure.

Figure 5 representing results of the EDS analysis for the Bi-rich alloy 6 (Bi0.8Sn0.2), shows the microstructure under low magnification (Fig. 5a) and high magnification with four different points for the analysis of the present phases (Fig. 5b).

As it is shown in Figure 5 and Table 4, the alloy 6 consists of bright, coarse dendrites of the Bi-rich solid solution and darker, interdendritic (Sn)+(Bi) eutectic regions. A good agreement between the chemical composition of the examined surface and the nominal alloy composition is obtained.

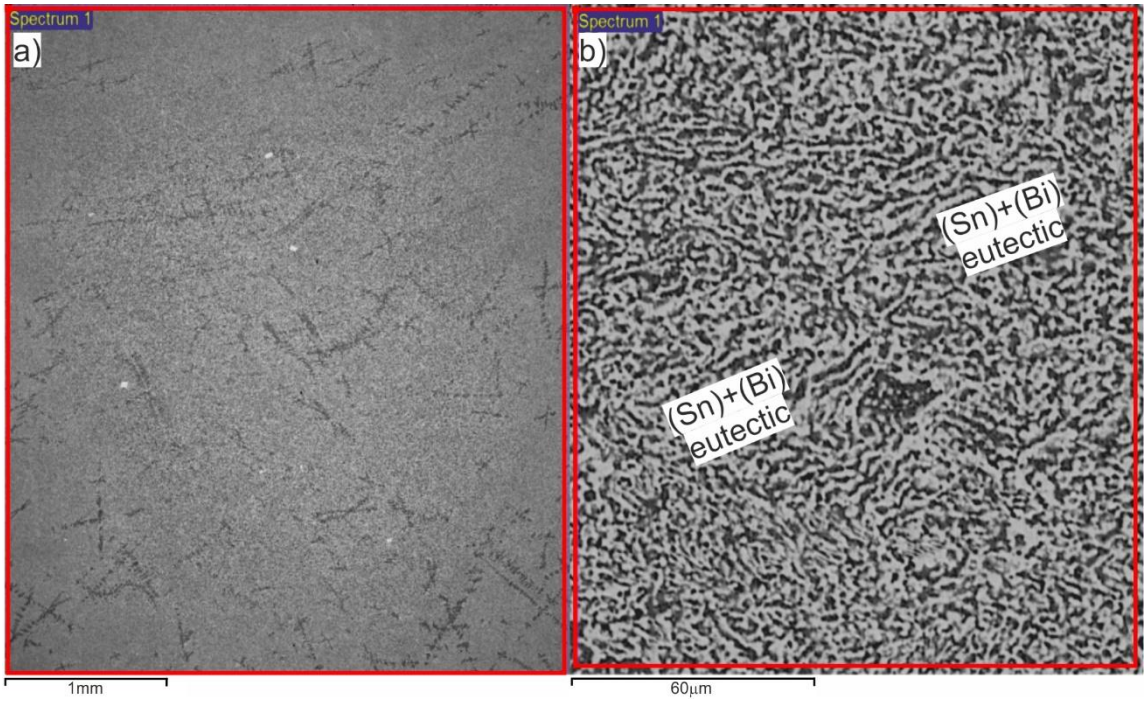

Fig. 4. SEM-EDS micrographs of the alloy 3 (Bi0.4Sn0.6): (a) determination of the overall composition; (b) determination of the composition of the eutectic microstructure

Table 3. Results of the EDS spectrum analysis for the alloy 3 (Bi0.4Sn0.6) showing the overall and the composition of the eutectic ((Sn)+(Bi)) mixture

Nominal composition of alloys, at%		Overall composition of the observed surface, at.%		Identified phase	Individual point spectrum	Content, at.%	
						Sn	Bi
Bi	Sn	Bi	Sn	(Sn)+(Bi) eutectic	Spectrum 1	60.72	39.28
40.00	60.00	39.14	60.86				

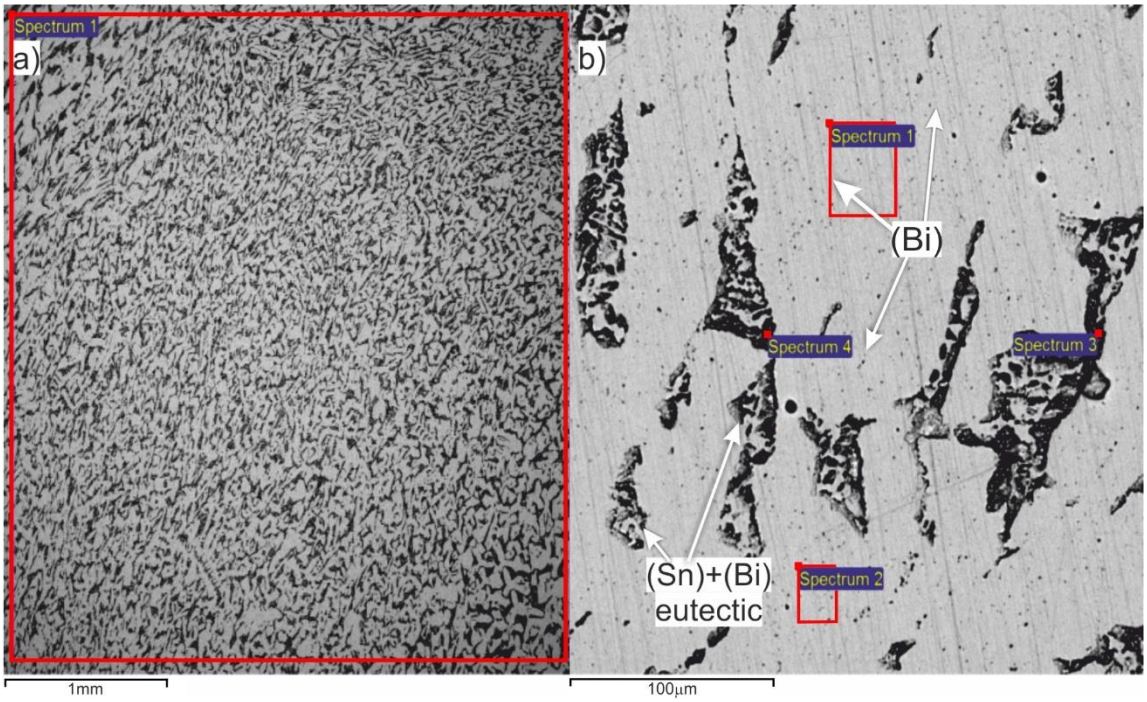

Fig. 5. SEM-EDS micrographs of the alloy 6 (Bi0.8Sn0.2): (a) determination of the overall composition; (b) determination of composition based on spectrums obtained at four different spots

Table 4. Results of EDS spectrum analyses for the alloy 6 (Bi0.8Sn0.2)

Nominal composition of alloys, at.%		Overall composition of the observed surface, at.%		Identified phase	Individual point spectrum	Content, at.%	
						Sn	Bi
Bi	Sn	Bi	Sn	(Bi)	Spectrum 1	2.56	97.44
					Spectrum 2	2.58	97.42
80.00	20.00	78.58	21.42	(Sn)+(Bi) eutectic	Spectrum 3	27.82	72.18
					Spectrum 4	46.43	53.57

The overall chemical compositions of the all prepared samples were checked by the EDS method and it was found that differences between the nominal and the experimentally determined compositions of alloys were negligible (less than 1 at.%).

3. 2. Hardness measurements

Hardness of the investigated alloys was determined by using the Brinell test method with the applied force of 50 N (Table 5). A decrease in hardness can be observed with addition of bismuth so that the largest hardness value was measured for the alloy 1. Similar results were observed in some previous studies [31].

Table 5. Hardness determined by using the Brinell test method at the force of 50N

Sample	Hardness, HB	
	Mean value	Standard deviation
Alloy 1	23.7	0.1
Alloy 2	22.4	0.4
Alloy 3	21.2	0.6
Alloy 4	20.0	0.4
Alloy 5	17.9	0.4
Alloy 6	18.0	0.4
Alloy 7	17.0	1.2
Pure Bi	10.7	0.2
Pure Sn	9.0	0.5

3. 3. DSC analysis

Melting behavior of the alloys was investigated by using differential scanning calorimetry (DSC) and results are given in Table 6 along with DSC thermograms in Figures 6-8, showing identified phase transition temperatures for the hypoeutectic alloy 2 (Bi0.2Sn0.8), near-eutectic alloy 3 (Bi0.4Sn0.6) and the hypereutectic alloy 6 (Bi0.8Sn0.2), respectively.

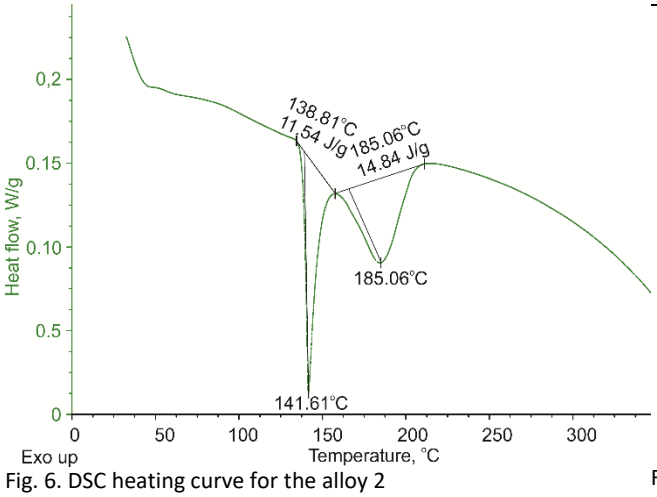

Fig. 6. DSC heating curve for the alloy 2

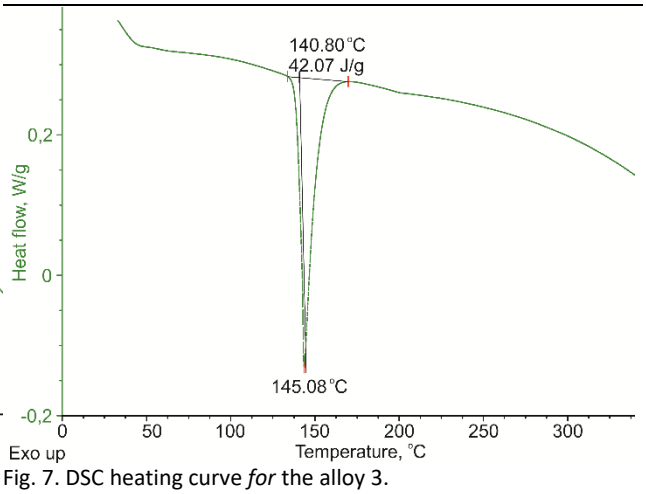

Fig. 7. DSC heating curve *for* the alloy 3.

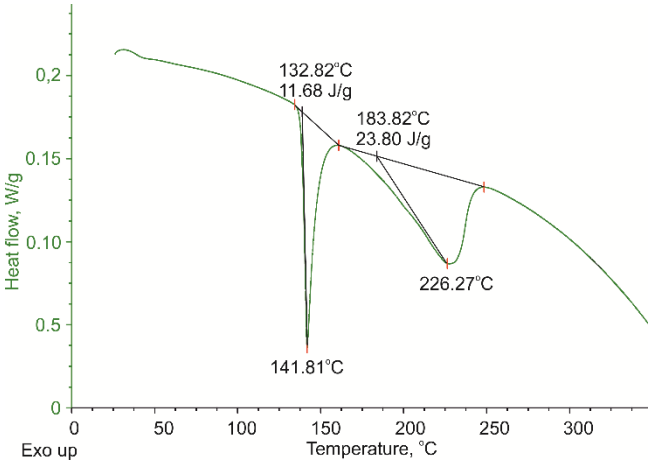

Fig. 8. DSC heating curve for the alloy 6

Table 6. Phase transitions temperatures for examined alloy compositions obtained by the DSC analysis

Sample	Phase transition temperature, °C	
	Eutectic reaction	Liquidus
Alloy 1	137.00	210.34
Alloy 2	138.80	185.00
Alloy 3	140.80	/
Alloy 4	139.73	171.11
Alloy 5	139.67	195.47
Alloy 6	138.82	226.27
Alloy 7	138.19	249.92

The obtained experimental results were compared to the results of thermodynamic calculations and good agreement was noticed. By using the COST 531 lead-free solder thermodynamic database [32] and the PANDAT software [33], a phase diagram for the Bi-Sn system was calculated (Fig. 9). Experimentally obtained results were inserted, where every square represents a temperature obtained by the DSC analysis, for a specific composition in the Sn-Bi system.

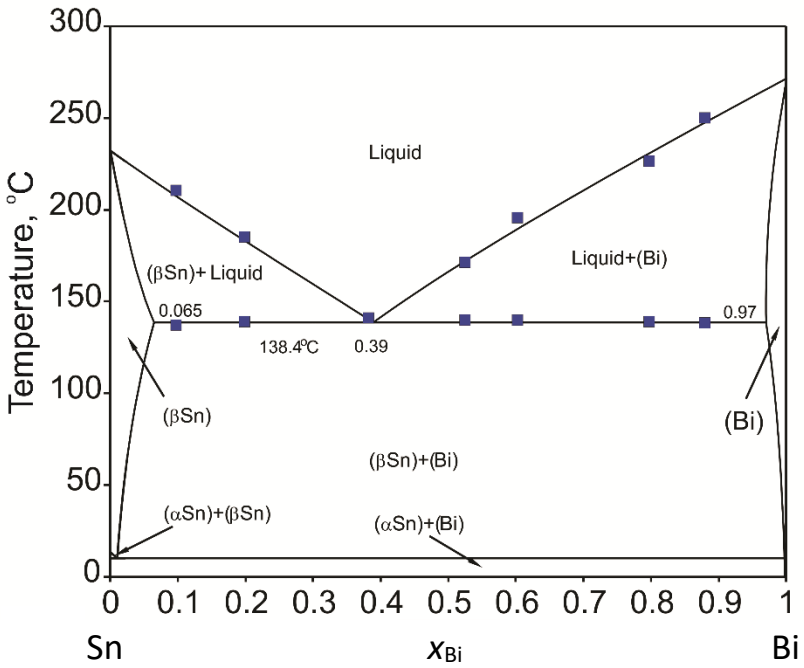

Figure 9. Calculated phase diagram of the Sn-Bi system by using the optimized thermodynamic parameters [32,34] and experimental results obtained in the present work (symbols)

Over the years, there were many uncertainties concerning the solvus surfaces of Bi and Sn in the Sn-Bi system. The uncertainties were mostly related to the Sn solvus surface, where the bismuth fraction went up to more than 10 at.% of bismuth in tin. In recent years, the solubility was calculated to be around 6.2 at.% [8]. In the present case, we confirmed that the solubility of Bi in tin was less than 10 at.%, and based on the calculated phase diagram using Pandat software [33], the solubility is around 6.5 at.%, which is in a good agreement with the proposed literature data.

3. 4. Thermal conductivity measurements

Thermal diffusivity and thermal conductivity were determined for every investigated Sn-Bi alloy composition by using the xenon-flash method [35]. Thermal conductivity of the investigated samples was determined by using the following fundamental relation (1):

$$\lambda = \alpha \, \rho \, C_p \tag{1}$$

where λ is the thermal conductivity, α is thermal diffusivity, ρ is density, and C_p is specific heat capacity. Thermal diffusivity was directly measured. Values of the specific heat capacity for the studied alloys were calculated by using the COST 531 thermodynamic database [32]. Alloys densities were determined by using the buoyancy method based on the Archimedes' principle. The results of conducted analyses are given in Table 7. The total uncertainty for the determined thermal conductivity is estimated to be ±8 % [30].

Table 7. Thermal diffusivities, specific heat capacities and thermal conductivities of the Bi-Sn alloys at 25, 50 and 100 °C.

Sample	t / °C	α / 10^{-4} m^2 s^{-1}		C_p / J g^{-1} K^{-1}	λ / W m^{-1} K^{-1}	
		Mean value	Standard deviation		Mean value	Standard deviation
Alloy 1	25	0.257	7.789	0.210	40.525	2.432
	50	0.253	7.594	0.213	40.337	2.420
	100	0.215	2.944	0.220	35.508	2.130
Alloy 2	25	0.172	9.274	0.195	26.161	1.570
	50	0.169	3.559	0.198	26.162	1.570
	100	0.148	2.082	0.204	23.597	1.416
Alloy 3	25	0.143	8.813	0.170	20.439	1.226
	50	0.143	2.887	0.173	20.683	1.241
	100	0.126	2.160	0.177	18.682	1.121
Alloy 4	25	0.125	7.416	0.160	19.764	1.186
	50	0.124	1.732	0.162	17.404	1.044
	100	0.110	2.887	0.166	15.852	0.951
Alloy 5	25	0.087	7.874	0.151	11.719	0.703
	50	0.089	8.832	0.153	12.065	0.724
	100	0.082	2.887	0.156	11.328	0.680
Alloy 6	25	0.057	1.000	0.135	7.231	0.434
	50	0.059	5.447	0.136	7.501	0.450
	100	0.057	1.732	0.139	7.484	0.449
Alloy 7	25	0.050	0.577	0.128	6.132	0.368
	50	0.051	1.732	0.129	6.341	0.380
	100	0.052	1.633	0.132	6.564	0.394

The obtained results show that the thermal diffusivity and thermal conductivity of the investigated Bi-Sn alloys gradually decrease with increasing the Bi content due to bismuth being one of the metals with the lowest thermal conductivity [36]. Figure 10 shows the dependence of the thermal conductivity on the alloy composition at 25 °C. The literature value of thermal conductivity for the commercial Bi58Sn42 (mas.%) solder alloy [37] is labeled in Figure 10 and used for comparison with the results obtained in the present study. A reasonable agreement can be observed. The specific heat capacity of the Sn-Bi alloys monotonically decreases with the increase in the Bi content (Fig. 11). It can be noticed that there is an excellent agreement of the calculated specific heat capacity in the present research with the value reported for the Bi58Sn42 (mas.%) solder alloy in literature [37].

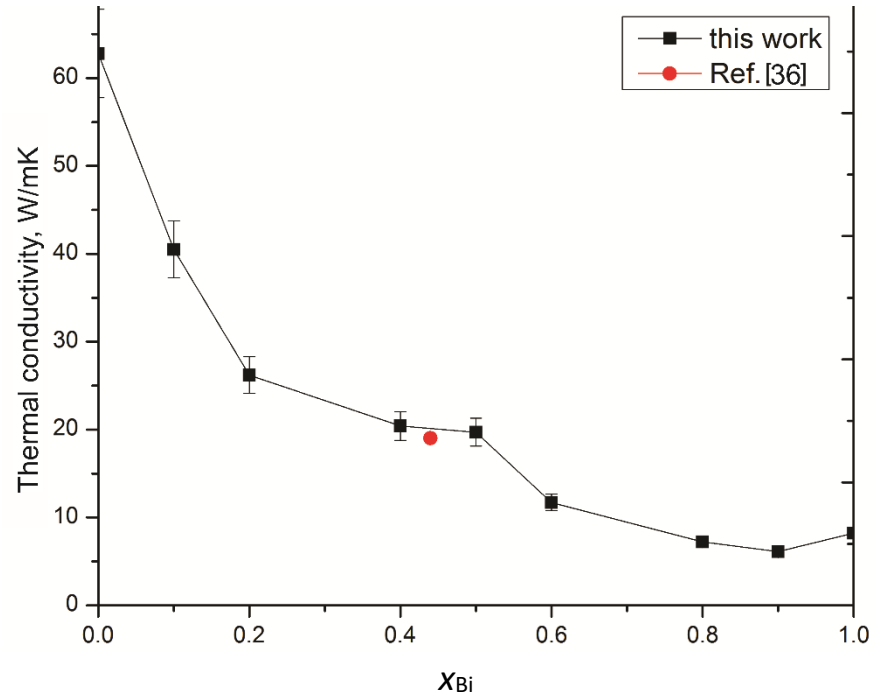

Fig. 10. Thermal conductivity of the Bi-Sn alloys at 25 °C as a function of alloy composition. Thermal conductivity values for pure Sn and Bi are from the ref. [38] while the red symbol shows the literature value for the commercial Bi58Sn42 (mas.%) solder alloy [37]

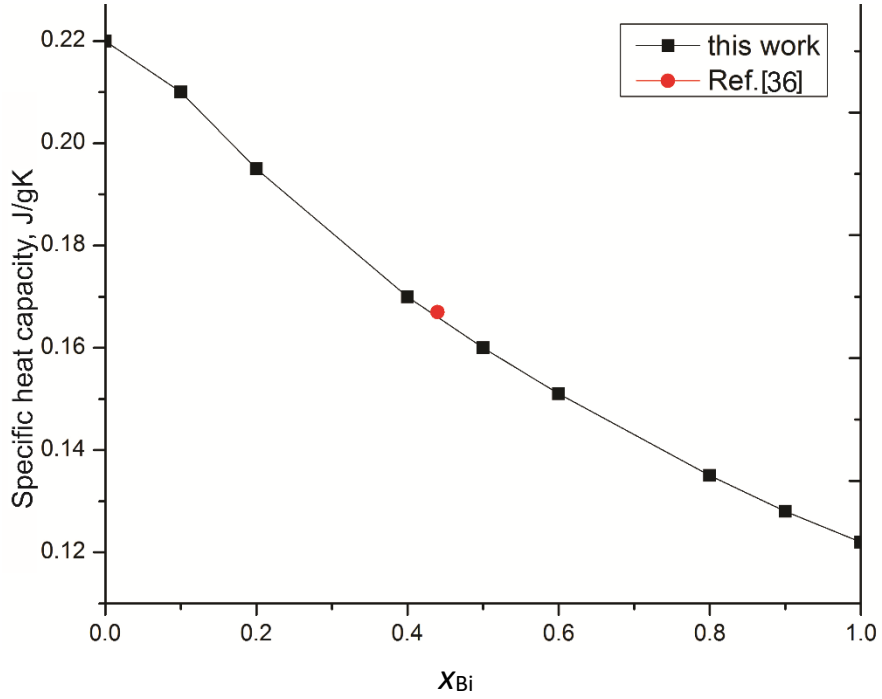

Fig. 11. Specific heat capacity of the Bi-Sn alloys at 25 °C as a function of alloy composition. Specific heat capacity values for pure Sn and Bi are from the ref. [38], while the red symbol shows the literature value for the commercial Bi58Sn42 (mas.%) solder alloy [37]

4. CONCLUSION

In this work, seven Sn-Bi alloys with bismuth molar fractions in the range from 0.1 - 0.9 were investigated regarding microstructure, hardness and thermal properties. Microstructural analyses performed by LOM and SEM- EDS have shown the existence of Sn-rich and Bi-rich solid solutions along with a complex regular eutectic microstructure

containing a mixture of (Sn) and (Bi) solution phases. Measured hardness values of the investigated Sn-Bi alloys were considerably higher than those of pure constitutive metals, Sn and Bi.

Using the optimized thermodynamic data from literature, a Sn-Bi phase diagram has been constructed. Furthermore, the phase transition temperatures, obtained by the DSC analysis, were compared to those in the phase diagram, and a good agreement was observed. Values of thermal diffusivity and thermal conductivity decreased with increasing the Bi content. The specific heat capacity also decreased with the increase in the Bi content and slightly increased with the increase in temperature. This work, focused on the investigation of thermal properties, hardness measurements and microstructure characterization of Sn-Bi alloys with different composition, provides a more detailed and attentive contribution to the general knowledge of this system.

Acknowledgements: The research presented in this paper was done with the financial support of the Ministry of Education, Science and Technological Development of the Republic of Serbia, within the funding of the scientific research work at the University of Belgrade, Technical Faculty in Bor, according to the contract under the registration number 451-03-9/2021-14/200131.

REFERENCES

[1] Frongia F, Pilloni M, Scano A, Ardu A, Cannas C, Musinu A, Borzone G, Delsante S, Novakovic R, Ennas G, Ennas. Synthesis and melting behaviour of Bi, Sn and Sn–Bi nanostructured alloy. *J. Alloys Compd.* 2015; 623: 7-14. https://doi.org/10.1016/j.jallcom.2014.08.122

[2] Ren G, Wilding I, Collins M. Alloying influences on low melt temperature SnZn and SnBi solder alloys for electronic interconnections. *J. Alloys Compd.* 2016; 665: 251-260. https://doi.org/10.1016/j.jallcom.2016.01.006

[3] Zhang X. P, Yu C. B, Zhang Y. P, Shrestha S, Dorn L. Processing treatment of a lead-free Sn–Ag–Cu–Bi solder by rapid laser-beam reflowing and the creep property of its soldered connection. *J. Mater. Process. Technol.* 2007; 192: 539-542. https://doi.org/10.1016/j.jmatprotec.2007.04.072

[4] Kanlayasiri K, Ariga T. Physical properties of Sn58Bi–xNi lead-free solder and its interfacial reaction with copper substrate. *Mater. Des.* 2015; 86: 371-378. https://doi.org/10.1016/j.matdes.2015.07.108

[5] Sun H, Li Q, Chan Y. A study of Ag additive methods by comparing mechanical properties between Sn57. 6Bi0. 4Ag and 0.4 wt% nano-Ag-doped Sn58Bi BGA solder joints. *J. Mater. Sci.: Mater. Electron.* 2014; 25: 4380-4390. https://doi.org/10.1007/s10854-014-2177-7

[6] Silva B, Garcia A, Spinelli J. Complex eutectic growth and Bi precipitation in ternary Sn-Bi-Cu and Sn-Bi-Ag alloys. *J. Alloys Compd.* 2017; 691: 600-605. https://doi.org/10.1016/j.jallcom.2016.09.003

[7] Abtew M, Selvaduray G. Lead-Free Solders in Microelectronics. *Mater. Sci. Eng.* 2000; 27: 95-141. https://doi.org/10.1016/S0927-796X(00)00010-3

[8] Braga M. H, Vizdal J, Kroupa A, Ferreira J, Soares D, Malheiros L. F. The experimental study of the Bi–Sn, Bi–Zn and Bi–Sn–Zn systems. *Calphad.* 2007; 31: 468–478. https://doi.org/10.1016/j.calphad.2007.04.004

[9] Mokhtari O, Nishikawa H. Correlation between microstructure and mechanical properties of Sn–Bi–X solders. *Mater. Sci. Eng.* 2016; 651: 831-839. https://doi.org/10.1016/j.msea.2015.11.038

[10] Zhao J, Qi L, Wang X, Wang L. Influence of Bi on microstructures evolution and mechanical properties in Sn–Ag–Cu lead-free solder. *J. Alloys Compd.* 2004; 375: 196-201. https://doi.org/10.1016/j.jallcom.2003.12.005

[11] Li J, Mannan S, Clode M, Whalley D, Hutt D. Interfacial reactions between molten Sn–Bi–X solders and Cu substrates for liquid solder interconnects. *Acta Mater.* 2006; 54: 2907-2922. https://doi.org/10.1016/j.actamat.2006.02.030

[12] Shen J, Pu Y, Yin H, Luo D, Chen J. Effects of minor Cu and Zn additions on the thermal, microstructure and tensile properties of Sn–Bi-based solder alloys. *J. Alloys Compd.* 2014; 614: 63-70. https://doi.org/10.1016/j.jallcom.2014.06.015

[13] Shalaby R. Effect of silver and indium addition on mechanical properties and indentation creep behavior of rapidly solidified Bi–Sn based lead-free solder alloys. *Mater. Sci. Eng., A.* 2013; 560: 86-95. https://doi.org/10.1016/j.msea.2012.09.038

[14] Miao H, Duh J. Microstructure evolution in Sn–Bi and Sn–Bi–Cu solder joints under thermal aging. *Mater. Chem. Phys.*. 2013; 71: 255-271. https://doi.org/10.1016/S0254-0584(01)00298-X

[15] Peng Y, Deng K. Fabrication of reduced graphene oxide nanosheets reinforced Sn–Bi nanocomposites by electro-chemical deposition. *Compos. Part A Appl. Sci. Manuf.* 2015; 73: 55–62. https://doi.org/10.1016/j.compositesa.2015.03.006

[16] Billah M, Chen Q. Thermal conductivity of Ni-coated MWCNT reinforced 70Sn-30Bi alloy. *Compos. B. Eng.* 2017; 129: 162-168. https://doi.org/10.1016/j.compositesb.2017.07.071

[17] Wang J, Wei H, He P, Lin T, Lu F. Microstructure and mechanical properties of tin-bismuth solder reinforced by aluminum borate whiskers. *J. Electron. Mater.* 2015; 44: 3872-3879. https://doi.org/10.1007/s11664-015-3896-0

[18] Peng Y, Deng K. Study on the mechanical properties of the novel Sn–Bi/Graphene nanocomposite by finite element simulation. *J. Alloys Compd.* 2015; 625: 44-51. https://doi.org/10.1016/j.jallcom.2014.11.110

[19] Lai Z, Ye D. Microstructure and fracture behavior of non eutectic Sn–Bi solder alloys. *J. Mater. Sci.: Mater. Electron.*2016; 27: 3182-3192. https://doi.org/10.1007/s10854-015-4143-4

[20] Silva B, Reinhart G, Nguyen-Thi H, Mangelinck-Noël N, Garcia A, Spinelli J. Microstructural development and mechanical properties of a near-eutectic directionally solidified Sn–Bi solder alloy. *Mater. Charact.* 2015; 107: 43-53. https://doi.org/10.1016/j.matchar.2015.06.026

[21] Gao L, Wang J, Lin T, He P, Lu F. Improvement of microstructure and mechanical properties of Sn-58Bi alloy with La_2O_3. In: *14th International Conference on Electronic Packaging Technology*. Dalian, China, 2013, pp. 193-195.

[22] Osório W, Peixoto L, Garcia L, Mangelinck-Noël N, Garcia A. Microstructure and mechanical properties of Sn–Bi, Sn–Ag and Sn–Zn lead-free solder alloys. *J. Alloys Compd.* 2013; 572: 97-106. https://doi.org/10.1016/j.jallcom.2013.03.234

[23] Guo Q, Zhao Z, Shen C. Comparison study on microstructure and mechanical properties of Sn-10Bi and Sn-Ag-Cu solder alloys and joints. *Microelectron Reliab.* 2017; 78: 72-79.

[24] Wang Q, Cheng X, Li Y, Yu G, Liu Z. Microstructures and Thermal Properties of Sn–Bi–Zn–Ga Alloys as Heat Transfer and Heat Storage Materials. *J. Wuhan Univ. Technol. Mater. Sci. Ed.* 2019; 34: 676-683. https://doi.org/10.1007/s11595-019-2103-1

[25] Wang F, Huang Y, ZhangZ, Yan C. Interfacial reaction and mechanical properties of Sn-Bi solder joints. *Mater.* 2017; 10: 920-936. https://doi.org/10.3390/ma10080920

[26] Hua F, Zequn M, Glazer J. Eutectic Sn-Bi as an alternative to Pb-free solders. In: *Proceedings of 48th Electronic Components and Technology Conference*. Seattle, Washington, 1998, pp. 277-283.

[27] Dong W, Shi Y, Xia Z, Lei Y, Guo F. Effects of trace amounts of rare earth additions on microstructure and properties of Sn-Bi-based solder alloy. *J. Electron. Mater*. 2008; 37: 982-991. https://doi.org/10.1007/s11664-008-0458-8

[28] Morando C, Fornaro O, Garbellini O, Palacio H. Thermal properties of Sn-based solder alloys. *J. Mater. Sci.: Mater. Electron.* 2014; 25: 3440-3447. https://doi.org/10.1007/s10854-014-2036-6

[29] Hu X, Li Y, Min Z. Interfacial reaction and growth behavior of IMCs layer between Sn–58Bi solders and a Cu substrate. *J. Mater. Sci.: Mater. Electron.* 2013; 24: 2027-2034 https://doi.org/10.1007/s10854-012-1052-7

[30] Manasijević D, Balanović Lj, Ćosović V, Minić D, Premović M, Gorgievski M, Stamenković U, Talijan N. Thermal characterization of the In–Sn–Zn eutectic alloy. *Metall. Mater. Eng*. 2019; 25: 325-334. https://doi.org/10.30544/456

[31] Marković B, Živković D, Manasijević D, Talijan N, Sokić M, Ćosović V. Phase Equilibria Calculation and Investigation of Hardness and Electrical Conductivity for Alloys in Selected Sections of Bi-Cu-Ni System. *J. powder metall. min.* 2012; 2:104 https://doi.org/10.4172/2168-9806.1000104

[32] Kroupa A, Dinsdale A, Watson A, Vrestal J, Vízdal J, Zemanova A. The development of the COST 531 lead-free solders thermodynamic database. *JOM*. 2007; 59: 20-25. https://doi.org/10.1007/s11837-007-0084-6

[33] Cao W, Chen S, Zhang F, Wu K, Yang Y, Chang Y, Schmid-Fetzer R, Oates W. PANDAT Software with PanEngine, PanOptimizer and PanPrecipitation for Multi-Component Phase Diagram Calculation and Materials Property Simulation. *Calphad*. 2009; 33: 328–342. https://doi.org/10.1016/j.calphad.2008.08.004

[34] Vízdal J, Braga M, Kroupa A, Richter K, Soares D, Malheiros L, Ferreira J. Thermodynamic assessment of the Bi–Sn–Zn System. *Calphad*. 2007; 31: 438-448. https://doi.org/10.1016/j.calphad.2007.05.002

[35] Parker W, Jenkins R, Butler C, Abbot G. Flash Method of Determining Thermal Diffusivity, Heat Capacity, and Thermal Conductivity. *J. Appl. Phys.* 1961; 32: 1679-84. https://doi.org/10.1063/1.1728417

[36] Engineering ToolBox, (2005). Thermal Conductivity of Metals, Metallic Elements and Alloys. [online] Available at: https://www.engineeringtoolbox.com/thermal-conductivity-metals-d_858.html. Accessed January 11, 2021.

[37] Indium Corp. Indalloy® 281 Bi-Sn Solder Alloy. http://www.matweb.com/search/datasheet.aspx?matguid=967a4cd7871b46fa9128a29c303cf8be. Accessed January 11, 2021.

[38] ASM Handbook Volume 2. *Properties and Selection: Nonferrous Alloys and Special-Purpose Materials*. ASM International; 1990.

SAŽETAK

Ispitivanje mikrostrukture, tvrdoće i termijskih karakteristika legura u sistemu Sn-Bi

Kristina N. Božinović, Dragan M. Manasijević, Ljubiša T. Balanović, Milan D. Gorgievski, Uroš S. Stamenković, Miljan S. Marković i Zoran D. Mladenović

Tehnički fakiltet u Boru, Odsek za metalurško inženjerstvo, Univerzitet u Beogradu, Vojske Jugoslavije 12, 19210 Bor, Srbija

(Naučni rad)

Zbog velike toksičnosti olova, bezolovni lemovi postali su glavni fokus elektronske industrije poslednjih godina. Zbog svojih povoljnih svojstava i niske cene, legure iz sistema Sn-Bi predstavljaju potencijalnu zamenu za legure Sn-Pb u lemljenju. Jedna od glavnih prednosti legura iz sistema Sn-Bi su niske temperature topljenja. Legure iz ovog sistema su takođe veoma atraktivne zbog dobre kompatibilnosti sa podlogama, niske temperature procesa, visoke pouzdanosti i potencijalne primene u vidu materijala termičkog sučelja. U ovom radu je urađena karakterizacija mikrostrukturnih i termijskih karakteristika, kao i merenje tvrdoće sedam Sn-Bi legura različitog sastava. Strukturna svojstva uzoraka analizirana su optičkom mikroskopijom i skenirajućom elektronskom mikroskopijom sa energetski disperzivnom spektrometrijom (SEM-EDS). Toplotna provodljivost uzoraka je ispitivana ksenon-fleš metodom (engl. xenon-flash method), a temperature faznih transformacija merene su diferencijalnom skenirajučom kalorimetrijom (engl. differential scanning calorimetry, DSC).

Ključne reči: strukturna svojstva; lemljenje; bezolovne lemne legure; toplotna provodljivost